ELSEVIER

Chemical Engineering Journal 137 (2008) 347–360

Chemical Engineering Journal

www.elsevier.com/locate/cej

A general model for analyzing data on the rate of reactive dissolution of poly-disperse particulate solids

Arijit Bhattacharya *

Chemical Engineering and Process Development Division, National Chemical Laboratory, 411008 Pune, India

Received 10 October 2006; received in revised form 5 April 2007; accepted 2 May 2007

Abstract

A model has been presented which successfully simulates the experimentally observed integral batch reactive dissolution rate data while accounting for the poly-dispersity of the solid particulate charge. This allowed avoiding arbitrary assumptions about the particulate inventory and size independence of the mass transfer coefficient. There is also no need for a priori identification of the controlling regime, which can change from kinetic to mass transfer during the process, apart from the possibility of the shift with the specified process and operating conditions. The model was applied with equal ease to a simple isothermal reaction, an exothermic reaction with runaway potential and to a phase-transfer catalysis reaction with a complex mechanism.

The model was shown to predict the time required for a specified extent of conversion of the particulate reactant or the rate of consumption of a key liquid reactant under a variety of process and operating conditions, like temperature, liquid reactant and the catalyst concentration, particle size, poly-dispersity of the charge and agitation speed. Such information is useful in reactor design and scale-up. Where dissolution is accompanied with a runaway reaction, the model can predict quantities of interest in hazard assessment and should aid safe reactor design.

Keywords: Reactive dissolution; Poly-disperse solid reactant; Particle size distribution; Solid–liquid PTC reaction; Reactive thermal hazard; Kinetic model

1. Introduction

Dissolution of solid reactants in a reactive liquid phase wherein the solute, following dissolution, reacts with one or more liquid reactant species, is an important unit process in the organic chemical process technology. For instance, in the production of terephthaloyl chloride, the reaction has been conducted [1] by suspending solid particles of terephthalic acid (TPA) in excess thionyl chloride ($SOCl_2$) in presence of dimethylformamide (DMFA). TPA from the surface of the particulate charge dissolves into the liquid phase where it reacts with $SOCl_2$ with DMFA serving as a catalyst.

$$1,4\text{-}C_6H_4(COOH)_2 + 2SOCl_2 \xrightarrow{(CAT)} 1,4\text{-}C_6H_4(COCl)_2 + 2HCl + 2SO_2$$

In view of the increasing awareness about the deleterious effect of solvents on the environment the trend in organic synthesis clearly favours reactions conducted in the above manner where one of the reactants acts as the solvent for the other which happens to be a solid under reaction conditions. There are a number of solid–liquid phase-transfer catalysed reactions (e.g., alkylation of the potassium salts of carboxylic acids such as benzoates, terephthalates by dissolving the solid salts in a neat liquid alkylating reactant such as *n*-octyl bromide [2]) reported in the literature that work on this principle.

In many hydrometallurgical processes of interest in mineral processing there are several examples of extraction of metal values from finely divided high grade concentrates, e.g., copper leaching from particulate chalcopyrite ores using hydrochloric or sulfuric acid under oxygen over-pressure [3]. There have been studies on dissolution of phosphatic minerals containing fluorapatite [4,5] in the production of phosphoric acid/phosphates for potential use in the fertilizer industry.

The kinetics of a wide variety of batch reactive dissolution processes arising in the above applications have often been studied in the laboratory by using a so-called 'mono-disperse' particulate charge that is at best one with a narrow particle size distribution (e.g., 80–120 μm of calcium oxide particles for its dissolution in aqueous HCl solutions [6]). The usual method of

* Tel.: +91 20 2590 2166; fax: +91 20 2590 2612.
E-mail address: a.bhattacharya@ncl.res.in.

1385-8947/$ – see front matter © 2007 Elsevier B.V. All rights reserved.
doi:10.1016/j.cej.2007.05.004

Nomenclature

a_{ls}	interfacial area for solid–liquid mass transfer (m^2)
A_1	frequency factor (($m^3\ kmol^{-1})^2\ s^{-1}$)
c_{vb}	specific heat of the calorimeter bomb/reactor ($kJ\ (g\ K)^{-1}$)
c_{vs}	specific heat of the reactor contents including solids ($kJ\ (g\ K)^{-1}$)
C	species concentration in the liquid phase ($kmol\ m^{-3}$)
C_0	initial solid loading ($kmol\ m^{-3}$)
D	solute diffusivity in solvent ($m^2\ s^{-1}$)
D_m	mean particle size (m or μm)
D_I	impeller diameter (m)
D_P	diameter of the spherical particles of a size group (m)
D_T	reactor diameter (m)
$\overline{D}$	parameter of the Rosin–Rammler type particle size distribution (m or μm)
E_1	activation energy ($kJ\ mol^{-1}$)
F	number distribution ($number\ m^{-1}$)
g	acceleration due to gravity ($m\ s^{-2}$)
h	impeller clearance (m)
H	liquid depth (m)
ΔH_r	heat of reaction ($kJ\ mol^{-1}$)
k_{ls}	solid–liquid mass transfer coefficient ($m\ s^{-1}$)
k_s	pseudo-first order reaction rate constant (s^{-1})
k_2	bimolecular reaction rate constant ($m^3\ kmol^{-1}\ s^{-1}$)
m_b	mass of calorimeter bomb/reactor (kg)
m_s	total mass of reactor contents including solids (kg)
M	instantaneous mass of the solid phase (kg)
MW	molecular weight
n	poly-dispersity index of Rosin–Rammler type distribution
N	agitation speed (rpm)
$R(D_P)$	'linear' dissolution rate ($m\ s^{-1}$)
R_g	universal gas constant
R_{RX}	rate of depletion of RX ($kmol\ m^{-3}\ s^{-1}$)
Re	Reynolds number
S	specific surface area of the initial solid charge ($m^2\ g^{-1}$)
S_L	percentage by weight of solids in the suspension
Sc	Schimdt number
Sh	Sherwood number
t	time (s)
T	temperature (K)
u_s	slip velocity ($m\ s^{-1}$)
u_t	terminal velocity ($m\ s^{-1}$)
V_l	liquid volume (m^3)
X	volume fraction distribution (volume fraction m^{-1})
Z_0	catalyst concentration ($kmol\ m^{-3}$)

Greek letters

φ	thermal inertia
μ	viscosity ($kg\ m^{-1}\ s^{-1}$)
ν	kinematic viscosity ($m^2\ s^{-1}$)
θ	t/τ
ρ	density ($kg\ m^{-3}$)
$\Delta\rho$	density difference ($kg\ m^{-3}$)
τ	time for specified extent of dissolution (s)
ω	fractional mass of remaining solid

Subscripts

A, B	liquid reactant species (e.g., thionyl chloride and ethyl acetate)
crit	lower limit of the agitation speed
Exp	experiment
H	higher limit of the particle size
l	liquid
L	lower limit of the particle size
Mono	mono-disperse (see Eq. (15))
MX, MY, QX, QY, RX, RY	species constituting the SLPTC reaction system
p	particle
s	solid solute
Sid	Sidorov (see Eq. (19))
0	initial

Superscripts

o	organic phase
*	saturation (interfacial)

interpretation of the laboratory rate data, whenever attempted (e.g., [1,6]), assumes that the remaining solid phase would continue to be effectively mono-disperse during dissolution, even as the characteristic particle diameter reduces. This entails a further assertion that the number of particles comprising the charge effectively remains the same during the process, which is not always true.

It has been shown by Leblanc and Fogler [7] and more recently by Bhattacharya [8] that during dissolution the particle size distribution of the remaining solid phase both widens and shifts along the size axis as a whole towards lower sizes. The assumption about the constancy of the poly-dispersity index of the distribution, therefore, is questionable. It can also be shown that except under differential conditions, the particle inventory in the course of dissolution is not necessarily conserved. Thus, though the extent of dissolution defined in terms of mass changes may not always reflect the error, the analysis has a lacunae that can potentially lead to erroneous results.

In any case the existing rate analysis methodology is not general enough to consider a case where the initial charge is distinctly poly-disperse. The particulate charge in many batch dissolution experiments have often been represented by an arithmetic average of the limits of the size group, e.g., in the case of dissolution of fluorapatite ores (size ranges of 1700–1400, 1180–1000, 850–710 and 600–550 μm by mean sizes 1550,

1090, 780 and 575 μm) in SO_2–water solutions [5]. Similar arithmetic mean sizes were used by Pradhan and Sharma [9] in presenting data on the dependence of the rate of PTC-assisted sulfidation of benzyl chloride on the particle size. There are elegant ways of characterizing the particle size distribution of these charges. Modern laboratory work/practice, increasingly, includes such data as a matter of routine. The interpretation of the dissolution rate data should also be compatible with and capable of using this additional information about the particulate charge.

Leblanc and Fogler [7] were the first to model the kinetics of batch dissolution of poly-disperse solids in a rigorous manner in the context of mineral processing. Unfortunately, the analysis was limited by restrictive assumptions of constant liquid phase concentration and about the controlling regime (mass transfer or pseudo-first order surface reaction). This allowed the authors to represent the intrinsic dependence of the solid–liquid mass transfer coefficient on the particle size in a simplistic manner.

In this paper, we present a simple and easy to use model for interpreting observed integral batch reactive dissolution rate data while accounting for the variation of the poly-dispersity of the solid phase and liquid composition during dissolution accompanied by reaction(s) in the liquid phase. It would be possible to specify in such a model the poly-dispersity of the charge as a measured information. The model will be initially developed for applications to simple isothermal reactions such as making terephthaloyl chloride referred to as above [1]. However, the model is consciously structured to allow, as shown later in the paper, easy extension to other organic synthesis reactions with a more complex mechanism as in the case of solid–liquid phase-transfer catalysis [9]. It will also be shown how by another minor extension, the model can be used to calculate the quantities of interest in reactive thermal hazard assessment should the dissolution process be followed by an exothermic runaway reaction in the liquid phase [10]. Interpretation of the rate data in such a wide range of reactive dissolution problems, of interest in the engineering of organic synthesis reactions, on the basis of a unified model does not seem to have been attempted before. Once validated the model would also help establishing the process sensitivity envelope that will be useful in the reactor design and scale-up.

2. Description of the basic model features

In what follows we describe the basic features of a mathematical model that represents the batch process of dissolution of a charge of particulate solids in a solution containing a predissolved reactant and/or a catalyst, which participate in an accompanying reaction to consume the dissolving solute and convert the same to desired product(s). The key assumptions underlying the analysis are:

1. The particulate charge is, in general, a poly-disperse one, characterized by a measurable particle size distribution.
2. The particle shape does not change significantly during the dissolution process and the particle 'size' can be based on the diameter of an 'equivalent' sphere having the same projected area as the particle.
3. The particles are substantially non-porous to start with and no porous solid product forms during the reaction.
4. There is no particle breakage by attrition, nor any growth by coalescence among particles.
5. The liquid medium is agitated by a mechanical stirrer, a minimum degree of agitation being mandated [11,12] for complete suspension of the particles depending upon the liquid and solid physicochemical properties, impeller design and placement ('clearance') and the solid loading.

2.1. Model equations

In the basic version of the model an isothermal pseudo-first order reaction is assumed to take place between the dissolving solute and the pre-existing reactant (with or without catalyst) in the liquid phase. It will be seen in the later part of the paper that the treatment can be generalised and extended to other more complex situations. Based on the above assumptions, following equations can be written using symbols defined in the nomenclature that will completely describe the model:

Particle mass balance

$$R(D_P) = \frac{dD_P}{dt} = -\frac{2MW_s k_{ls}(C_s^* - C_s)}{\rho_s} \quad (1)$$

Particle population balance

$$\frac{\partial F(D_P, t)}{\partial t} = -\frac{\partial}{\partial D_P}[R(D_P)F(D_P, t)] \quad (2)$$

where $F(D_P, t)\Delta D_P$ is the number distribution of the particles, denotes the number of particles belonging to the sizes between D_P and $D_P + \Delta D_P$. At the start of the process (i.e., $t = 0$) one specifies an initial particle size distribution, $F(D_P, 0)$.
Mass balance for the dissolved solid species

$$V_l \frac{dC_s}{dt} = \sum_{D_{PL}}^{D_{PH}} k_{ls} a_{ls}(C_s^* - C_s) - V_l k_s C_s \quad (3)$$

with the initial condition (at $t = 0$) set as $C_s = 0$ and the apparent rate constant being expressed as

$$k_s = k_2 Z_0 \quad (4)$$

and the surface area of the particles in a given size group as

$$a_{ls} = \frac{6X(D_P, t)\Delta D_P M_s}{\rho_s D_P} \quad (5)$$

with

$$M_s = \frac{\pi \rho_s}{6} \sum_{D_{PL}}^{D_{PH}} D_P^3 F(D_P, t)\Delta D_P \quad (6)$$

2.2. Solid–liquid mass transfer coefficient

This parameter is usually correlated with particle size, agitation speed and properties like density of the solid and the liquid,

viscosity of the liquid and the diffusivity of the dissolving solute species in the liquid phase. Under conditions where the particles are fully suspended in the liquid phase, one general way of representing such a correlation, that may yield a conservative estimate of k_{ls}, is a form of modified Frössling relationship, namely,

$$Sh_p = 2 + \chi(Re_p)^{\beta}(Sc)^{\gamma} \quad (7)$$

The first term on the right hand side of the equality sign occurs due to the asymptotic molecular diffusion contribution that has been experimentally proven [17] to a large extent and also has some theoretical justification [18]. It is in the form of the turbulent contribution (the second term on the RHS) that some variability exists and a plethora of correlations [13–17] have been proposed varying in the values of the coefficient χ and the exponents β and γ. In one of the more recent and carefully conducted experimental studies of mass transfer to 6–420 μm diameter ion-exchange particles from aqueous glycerol solutions, Armenante and Kirwan [17] had found that $\chi = 0.891$, $\beta = 0.329$ and $\gamma = 0.333$. We used this correlation, with appropriate accounting of the physical property variations, being well suited to the particle size range in many solid–liquid reaction experiments of interest in this work. Thus, k_{ls} could be estimated using the following equation:

$$k_{ls} = \left(\frac{D}{D_P}\right)\left[2 + 0.891\left(\frac{D_P u_s \rho_l}{\mu_l}\right)^{0.329}\left(\frac{\mu_l}{\rho_l D}\right)^{0.333}\right] \quad (8)$$

The 'slip' velocity (in the above equation) was correlated with the terminal velocity of the particles as suggested by Miller [16].

$$u_s = 0.000644 N^{1.239} u_t, \quad N \geq N_{crit} \quad (9)$$

where N_{crit} represents the minimum agitation speed at which all the particles are suspended. In the above particle size range the terminal velocity, in turn, can be computed from the equation originally used by Harriot [13] and recommended by others [19].

$$u_t = \frac{0.153 g^{0.71} D_P^{1.14} \Delta\rho^{0.71}}{\rho_l^{0.29} \mu_l^{0.43}} \quad (10)$$

The Eqs. (8)–(10) were used in this work to predict k_{ls} variation with the particle diameter for the specified physicochemical properties. The minimum agitation speed for complete particle suspension, as proposed by Zwietering [11], can be conveniently calculated by the following equation as given by Nienow [12]

$$N_{crit} = \frac{s \nu_l^{0.1} D_P^{0.2} (g\Delta\rho/\rho_l)^{0.45} S_L^{0.13}}{D_I^{0.85}} \quad (11)$$

Nienow [12] has provided a graph to evaluate the factor s for specified ratio of the reactor-to-impeller diameters (D_T/D_I) and the impeller clearance ratio (h/H). For instance, for a typical case of $D_T/D_I = 2.5$ and $h/H = 1/5$, $s = 5.25$. A recommended value for the former ratio is 3 and that for the later is 1/6. It can be shown that using a stirring speed greater than N_{crit} does not increase k_{ls} significantly. However, wherever experimental conditions specified a speed that was greater than N_{crit} it was used in the calculation.

2.3. Solution procedure

Eqs. (2) and (3) as set out above will have to be solved simultaneously to calculate the number distribution of the particles $F(D_P, t)$ and the dissolving solute species concentration C_s in the liquid phase as functions of time. Eq. (1) provides the intrinsic rate of decrease in the diameter of the particles in each size group (which may be termed as the 'linear' dissolution rate in analogy to the expression linear growth rate in crystallization) as required in the Eq. (2). Eqs. (4)–(6) and (8)–(10) provide the necessary expressions for quantities required to be evaluated within Eq. (3).

By choosing to represent the k_{ls} dependence on size by a power law expression and assuming a large (relatively unchanging) liquid reagent (solvent) concentration, Leblanc and Fogler [7] had combined Eqs. (1) and (2) and disregarded the Eq. (3). The resulting partial differential equation was analytically solved by the method of characteristics. The solution required definition of a specific analytic form of both the initial and the final particle size distribution of the solid charge (such as log–normal or Rosin–Rammler). Thus, the analytical approach, though feasible appears more suited to applications involving differential rate data. The power law representation for the 'linear' dissolution rate (based on simplified analytic form of the k_{ls} expression) is, in general, not justified. The assumption of constant liquid composition would further restrict the scope of application of the model especially in the context of the present paper.

In the procedure devised in this work, the size distribution function was discretised by a simple finite difference scheme over the size space, which was divided into N_D equal size intervals within the lower and upper limits, D_{PL} and D_{PH}, respectively. Choosing a forward difference scheme Eq. (2) can be written for a size group containing particles having diameters between D_P and $D_P + \Delta D_P$ as

$$\frac{\partial[F(D_P, t)\Delta D_P]}{\partial t} = R(D_P)F(D_P, t) - R(D_P + \Delta D_P) \times F(D_P + \Delta D_P, t) \quad (12)$$

This equation on recurrent application to each group would provide N_D equations and those along with the Eq. (3) can be solved simultaneously as a set of ordinary differential equations (ODE) by using a standard ODE solver. Such a discretisation method was also used successfully by Adrover et al. [20] in a related problem (fragmentation or 'sporulation' of oxide grains from the particles of a manganiferrous ore along with dissolution of released grains in acidic solutions) for solving a similar set of equations numerically We used in this work the ODE solver IVPAG from the Visual Numeric's IMSL mathematical subroutines package. This Eulerian discretisation was found efficient and adequate for the present problem. More complicated and implicit discretisation schemes are possible and were tried but the accuracy was not significantly increased, but the computational effort escalated greatly. The computed results did show some sensitivity with respect

to the choice of N_D. However, the results remained invariant beyond $N_D = 100$ which was used in all subsequent calculations.

It is important to note that the procedure devised and used here completely frees one from any restriction on the form of the 'linear' dissolution rate R, which is process specific and, in general, need not have a closed form expression (such as a power law form). Indeed it may not even be analytic under some conditions and may have to be computed only numerically as it will be shown in the context of other more complex reactions to be considered in course of the paper.

As a test of the accuracy of the above procedure the model predicted rate of dissolution of potassium sulfate in water were compared against that obtained by the analytical approach. The properties data for the system were taken from Ditl et al. [21]. By holding the dissolved salt concentration at a constant level (large solvent volume) the concentration driving force became constant. By using Calderbank and Moo-Young correlation [14] for the K_2SO_4–water system over a particle size range 50–250 μm and an agitation speed in the range of 500–700 rpm the k_{ls}–D_P power law relationship can be shown to be represented as

$$k_{ls} = 5.573 \times 10^{-5} D_P^{-0.1154} \tag{13}$$

Eq. (13) evaluates k_{ls} at 232×10^{-6} m to be 1.464×10^{-4} m/s while Ditl et al. [21] reported the value to be 1.455×10^{-4} m/s. The particle size distribution of the initial charge was specified in terms of a volume fraction distribution of the Rosin–Rammler type:

$$X(D_P, 0) = \frac{n}{\overline{D}} \left(\frac{D_P}{\overline{D}} \right)^{n-1} \exp\left[-\left(\frac{D_P}{\overline{D}} \right)^{n} \right] \tag{14}$$

With a poly-dispersity index (denoting the degree of poly-dispersity of the material) $n = 21$ and the mean statistical diameter (a measure of the material fineness) $\overline{D} = 232 \times 10^{-6}$ m, the analytical expression due to Leblanc and Fogler [7] was used to calculate (the procedure has been demonstrated by Bhattacharya [8]) the variation of the extent of dissolution with time. The time scale was converted to a dimensionless one (θ) using time required for 90% dissolution as the normalizing parameter. The extent of dissolution has been represented as the fractional mass of the solids remaining (ω). The same profile was also computed by the numerical procedure proposed in the present work for the same initial solid charge and using the same property values, this time using the Calderbank and Moo-Young correlation directly without making any approximation such as Eq. (13). Being a case of physical dissolution k_s was set to zero in the Eq. (3). Fig. 1 compares the two profiles. There is hardly any discrepancy in the numerical results. In what follows the model and the numerical solution procedure is further validated by applications to reactive systems.

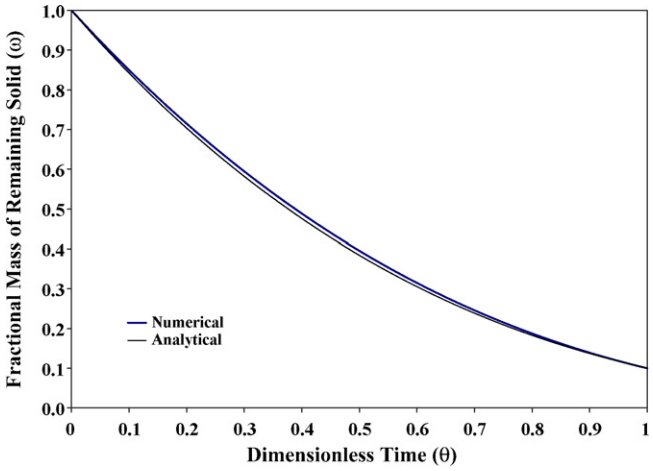

Fig. 1. Comparison of the predicted rate of dissolution of potassium sulfate in water by the numerical and the analytical approaches.

3. Application of the model: reaction between terephthalic acid and thionyl chloride in presence of dimethylformamide

3.1. Comparison with the observed dissolution rates

Particulate terephthalic acid (TPA) suspended in excess thionyl chloride ($SOCl_2$) dissolves and this dissolution is accompanied by the reaction between TPA and $SOCl_2$ to produce a liquid product terephthaloyl chloride and also sulfur dioxide and hydrochloric acid gases (see Section 1). While this reaction is known to proceed without any catalyst, albeit very slowly, presence of a small amount of dissolved dimethylformamide (DMFA) catalyses the reaction considerably. In view of the usually large mole ratios between $SOCl_2$ and TPA and presence of DMFA in catalytic amounts, the reaction kinetics can be taken as effectively first order in TPA concentration with the DMFA concentration included in the pseudo-first order reaction rate constant.

TPA dissolution rates under a variety of process and operating conditions were systematically studied experimentally by Sidorov et al. [1] and the reaction kinetics reported in the same paper. To interpret the data the authors made an analysis of the diffusional mass transfer of TPA from the surface of the TPA spheres of uniform size into the $SOCl_2$–DMFA liquid solution accompanied by a pseudo-first order reaction in the liquid phase. An important quantity resulting from this analysis was the time required for complete dissolution of TPA particles. For the convenience of the presentation and discussion of the results, we reproduce without derivation the following expressions given by Sidorov et al. [1]:

$$\tau_{Mono} = \frac{3(\alpha + 1)}{b(C_s^*)\alpha} \tag{15}$$

where

$$\alpha = \frac{3k_s}{bC_0} \tag{16}$$

and

$$b = \frac{6\mathrm{MW_s}k_{ls}}{\rho_s D_{P0}} \tag{17}$$

This simplified analysis, however, was bound by an implicit assumption that the remaining particulate phase continues to be essentially mono-disperse at all times during the entire dissolution period which is unlikely to be true. The authors also assumed a size-independent (constant) solid–liquid mass transfer coefficient. In the small particle size range pertinent to the experimental data in question (<100 μm), k_{ls} could in principle vary almost inversely with the particle diameter. In the previous section we have reanalyzed the problem accounting for the poly-dispersity of the solid phase and without having to make any assumption about the transport coefficient.

The new model has been used to calculate the time required for dissolving the solid charge to different extents (TPA conversion in the parlance of the paper) under conditions as specified for the so-called "control experiments" (Table 1 of their paper [1]). In these experiments, the reactant/catalyst mol ratio was maintained constant, but the reaction temperature, the extent of TPA conversion and the specific surface area were varied. These being generally poly-disperse charges the equivalent starting mean particle diameter was calculated from the measured specific surface area in each case by using the following expression:

$$D_{P0} = \frac{6}{S\rho_s\sigma} \tag{18}$$

where σ is a shape factor whose value was specified by the authors to be 0.35. However, instead of using the Eq. (15), Sidorov et al. presented another empirically correlated expression for the time for complete conversion:

$$\tau_{Sid} = \frac{(C_0 D_{P0})^{0.5}}{k_2 Z_0^{0.75}} \tag{19}$$

with the rate constant correlated by the following Arrhenius equation:

$$k_2 = \exp\left[30.57 - \frac{5.9}{R_g T}\right] \tag{20}$$

In trying to apply our model to these data we used the same rate constant expression as above, the mole ratio and the temperatures as specified in the experiments. The initial particle size distribution was specified in terms of a volume fraction distribution of the Rosin–Rammler type such as given by Eq. (14).

The distribution parameters n and $\overline{D}$ were chosen so as to closely approximate the measured specific surface area for a given initial charge. For instance, for the cases 1 and 2, an initial charge with $n = 9$ and $\overline{D} = 60\,\mu\mathrm{m}$ gave a specific surface area of about $0.2023\,\mathrm{m^2/g}$, close to $0.2\,\mathrm{m^2/g}$ that was used in the experiments. k_{ls} was calculated by the Eq. (8).

The density of TPA and that of $SOCl_2$ and the viscosity of the latter were taken from the published data in the handbooks, property compendia [22–24] and encyclopedia [25]. The diffusivity of TPA in $SOCl_2$ solutions was calculated by using the Wilke–Chang correlation [21]. The solubility of TPA in $SOCl_2$ has not been reported in the literature, nor was it measured by Sidorov et al. [1]. It is understandable that the measurement is complicated because of slow non-catalytic reaction between the solute and the solvent. Moreover, TPA solubility might be affected further in presence of DMFA [25]. For this set of data, the solubility value could be back calculated using the Eq. (15) and was found to vary between 0.29 and $0.98\,\mathrm{kmol\,m^{-3}}$ with an average of four values being $\sim 0.515\,\mathrm{kmol\,m^{-3}}$. We found that a value $0.55\,\mathrm{kmol\,m^{-3}}$ gave the best fit of the entire data set.

With all the above data having been available the model could be used to calculate the time required to achieve a given extent of TPA conversion. The predicted values for τ (and for $\tau_{0.5}$ as the case may be) for all the six cases have been compared in Table 1 with the reported experimental values as well as against the values calculated both by the "mono-disperse particles model", Eq. (15) or the "mono-model" (as an abbreviation by which we would refer to it henceforth), and by the empirical formula given by the Eq. (19). In the last row of this table we present the model predicted τ for another run reported elsewhere in the same paper [1] that used about the same mole ratios as in the other six cases, but the initial charge was essentially a mono-disperse one. The calculations were set up and performed in the same way as for the other cases, the only difference being that the value for n was set to be much higher ($n = 21$) to approximate the mono-disperse nature of the initial distribution, and $\overline{D}$ taken to be the same as the stated initial mean particle size. It was found that using still higher n did not materially affect the results.

It is to be noted that in six out of the seven cases considered, the model predicted values are closer to the experimental ones than those predicted by the mono-model, which always overpredicts and in some cases appreciably. The empirical Sidorov formula (Eq. (19)) predicted better than the mono-model but in

Table 1
Comparison of the predicted times for specified TPA conversion for several TPA charges with the observed ones under various experimental conditions [1]

Temperature (°C)	Specific surface area of charge ($\mathrm{m^2\,g^{-1}}$)	Z_0 ($\mathrm{kmol\,m^{-3}}$)	C_0 ($\mathrm{kmol\,m^{-3}}$)	n	$\bar{D}$ ($\times 10^6$ m)	TPA conversion (%)	τ_{exp} (h)	τ (h)	τ_{Mono} (Eq. (15); h)	τ_{Sid} (Eq. (19); h)
60	0.202	0.262	2.48	9	60	50	2.43	1.71	2.47	2.42
70	0.202	0.262	2.48	9	60	100	3.25	3.12	3.53	4.00
60	0.899	0.262	2.48	9	13.5	50	1.44	1.20	2.06	1.14
70	0.899	0.262	2.48	9	13.5	100	1.17	1.35	1.54	1.91
60	4.496	0.262	2.48	9	2.7	100	2.92	3.12	4.06	2.54
65	4.496	0.262	2.48	9	2.7	100	1.33	1.80	2.34	1.45
70	0.773	0.194	2.48	21	15	100	1.80	1.76	2.06	1.66

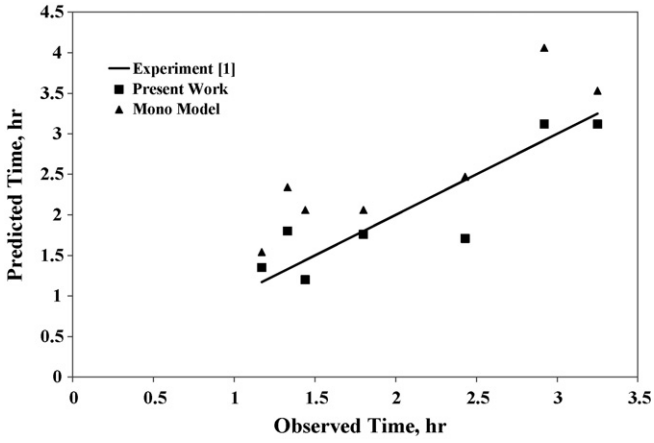

Fig. 2. Comparison of the observed and the predicted time for specified conversion of TPA under various conditions.

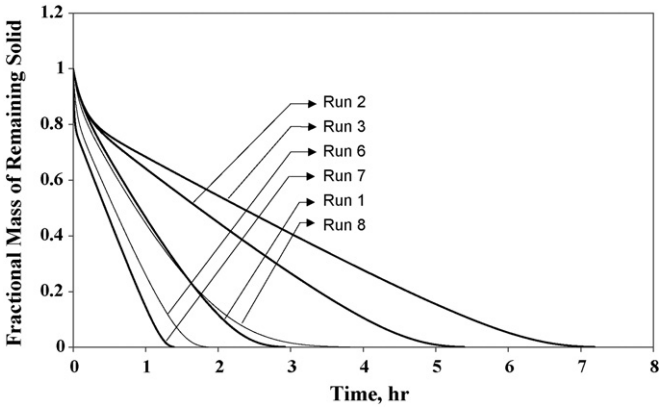

Fig. 3. Sensitivity of the rate of dissolution vis à vis process and operating variables.

most cases not better than our model. Moreover, being empirical the utility of this formula is very limited. Thus, the model presented in this work, apart from being theoretically more sound, is more consistent and accurate among the three predictive options available in this case. The model can handle both poly-disperse and mono-disperse charges with equal ease. Fig. 2 shows a parity plot between the observed and predicted times for all these seven cases.

In the above form of application the model was used in an almost predictive manner wherein the kinetics was specified, the mass transfer coefficient calculated by a published correlation, most physicochemical data taken from handbooks. It was only the TPA solubility value that was somewhat uncertain. Another way to utilize the model was to use it in conjunction with the measured rate data such as above for estimating the kinetic (Arrhenius) parameters and solubility (for which experimental or reported value was not available). These parameters were re-estimated using a standard optimization module BCLSF from the IMSL library (Visual Numerics) and virtually the same values as used above were obtained.

3.2. Sensitivity of the dissolution rate towards process and operating conditions

We have shown that the model could display correct response to changes in some of the process and operating conditions as in the control experiment runs of Sidorov et al. [1]. We then made a systematic study of the sensitivity of the model to some of the common and the pertinent process and operating variables that a process developer would normally like to vary which could provide necessary guidelines in planning and conducting such reactions for research and/or development purpose. Ten such conceptual runs were studied numerically with the help of the model and using the same data and parameters as above and are summarized in Table 2. The second through seventh columns of this table contain the values set for each of these variables. The last three columns summarise the time required for complete dissolution of the solid charge calculated by the new model vis à vis the values computed by the mono-model and the empirical Sidorov formula.

The first run (the base case) considers a mono-disperse charge at the temperature and catalyst concentration as used in the run 2 of the "control experiments" (see Table 1). The next three runs involve the effect of temperature and/or catalyst concentration (keeping all other variables the same as in the base case) on the rate indicating that the overall rate, in this problem, is quite strongly dependent on the kinetic factors (with the effect of catalyst concentration being stronger than that of temperature, see the Run 4 results in Table 2). The same trend would show up clearly on a fractional mass of the remaining solid versus time plot (Fig. 3).

Table 2
Predicted variation of the time for complete dissolution of specified particulate charges under various process and operating conditions

Run no.	Temperature (°C)	Mole ratio	Z_0 (kmol m^{-3})	C_0 (kmol m^{-3})	n	$\bar{D}$ ($\times 10^6$ m)	N_{crit} (rpm)	τ (h)	τ_{Mono} (Eq. (15); h)	τ_{Sid} (Eq. (19); h)
1	70	1:4:0.078	0.262	2.48	21	60	500	2.92	3.53	2.64
2	60	1:4:0.078	0.264	2.48	21	60	500	5.39	6.21	7.83
3	70	1:27.9:0.12	0.059	2.48	21	60	500	7.19	8.25	8.11
4	65	1:27.9:1.0	0.473	2.48	21	60	500	2.85	3.45	2.90
5	70	1:4:0.078	0.262	2.48	9	60	500	3.12	3.53	2.64
6	70	1:4:0.078	0.262	2.48	9	30	500	1.86	2.06	1.87
7	70	1:4:0.078	0.262	2.48	9	15	500	1.39	1.58	1.32
8	70	1:4:0.078	0.262	2.48	4	60	500	3.82	3.53	2.64
9	70	1:4:0.078	0.262	2.48	9	60	700	2.99	3.36	2.64
10	70	1:4:0.078	0.262	2.48	9	60	350	3.25	3.71	2.64

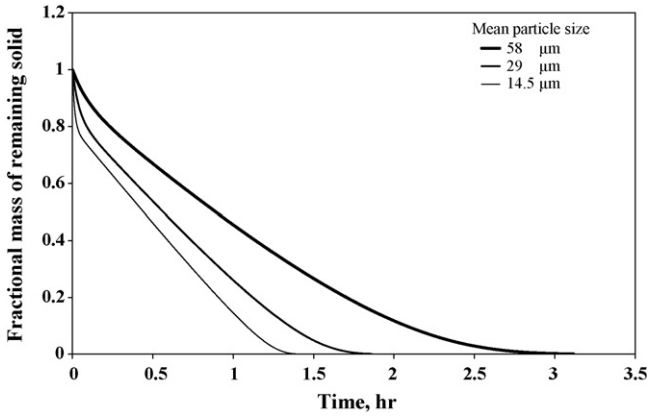

Fig. 4. Effect of particle size on the extent of dissolution.

Run nos. 5, 6 and 7 demonstrate the expected effect of reducing mean particle size of the initial solid charge (at a given poly-dispersity, i.e., constant n), namely, increased rate of dissolution. The mean particle size has been calculated by the following formula valid for the Rosin–Rammler distribution assumed here for the charges:

$$D_{\mathrm{m}} = \bar{D}(\ln 2)^{(1/n)} \tag{21}$$

What should be noticed, however, is that as the particle size is reduced the rate curves (see Fig. 4) approach an asymptotic profile implying the kinetic control. Thus, reducing the mean particle size below a certain level may not yield much rate enhancement.

Run nos. 1, 5 and 8 together show the effect of poly-dispersity of the charge (n) on the rate (for identical $\overline{D}$ and with all other variables kept constant). We observe that an increase in the poly-dispersity clearly increases τ. The interesting point to note (compare the plots for run nos. 1 and 8 in Fig. 3), however, is that for the first 40–50% dissolution, the poly-disperse charge dissolves at a faster rate than a mono-disperse one, while in the latter half of the conversion history the trend is exactly the reverse. This observation can be rationalized in terms of Fig. 5, where it can be seen that initially a poly-disperse charge provides a greater specific surface area than a mono-disperse one. But as

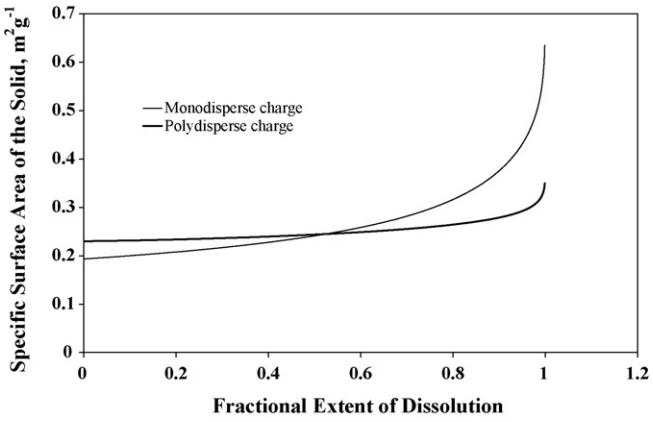

Fig. 5. Effect of poly-dispersity of the charge on the specific surface area of the solid phase.

the dissolution progresses, the latter moves rapidly to the lower particle size range with a large enhancement in the specific surface area, whereas for the former charge the change in the particle size distribution is relatively marginal thereby limiting the rise in surface area with time. For the simple isothermal first order reaction considered above this may not make much difference, but in the case of exothermic reactions or complex secondary reactions in the liquid phase, the difference may become significant in some cases.

Runs 5, 9 and 10 (see Table 2) show the effect of agitation speed on the rate. As expected this variable, which mainly affects the mass transfer coefficient (that too in a sub-linear manner), would not significantly affect the rate, especially as the rate of reaction, for this particular problem, is not essentially mass transfer controlled. However, it was important to make sure that for the given charge and loading conditions the agitation speed is larger than N_{crit}. This value was 336 rpm in the present case. Thus, in general, where the kinetic factors play substantial role, the agitation speed should be chosen well above N_{crit} but variation in this variable is not likely to be important.

4. Extension of the model to exothermic reactions

4.1. Simulation of the self-heating in a runaway reaction

A natural extension of the model presented earlier is to the case of solid dissolution followed by an exothermic reaction in the liquid phase. In many multiphase reactions studied or used for the development of fine and speciality chemicals the issue of thermal runaway hazards (with accompanying gas evolution leading to rupture of the containment chambers) is very real. Correct estimates of the adiabatic (or the maximum) temperature rise, the maximum self-heating rate, the time-to-maximum rate (TMR) and the temperature at the maximum rate (TeMR) in the context of the batch operation of test reactors, calorimeters (e.g., accelerated rate calorimeter or ARC) carrying out such a reaction are useful for safe reactor design and scale-up.

In course of an investigation into the thermal runaway occurring in a drum storing a mixture of thionyl chloride and ethyl acetate, Wang et al. [10] found that dissolution of the zinc coating on the steel drum followed by a highly exothermic reaction was the cause of the runaway. As a part of their studies on the compatibility of liquid mixture with the material of construction of the drum, they conducted tests in an ARC and in a number of small-scale adiabatic reactors holding the mixture and loading into it either drum scrapings, galvanized strips of metal or fine zinc powder. In each case, a runaway was invariably observed after a short time period, with variable heat generation and pressurization rates. Although the context is indirect, this provided a good, realistic experimental study of the heat generation and a very rapid temperature rise attendant on an exothermic reaction following dissolution of a mass of fine powdered solid in a reactive liquid medium. This was a fit case to which our model could be applied.

The model described earlier will have to be slightly extended and generalised to become applicable to this problem. Although the reaction following the dissolution of metallic zinc may

be a multi-step one and involves radicals or intermediates, for the present purpose we would assume it to proceed as follows

$$\mathrm{Zn(s)} + \mathrm{SOCl_2(l)} + \mathrm{C_2H_5COOCH_3(l)} \rightarrow \mathrm{SO_2(g)} + \mathrm{C_2H_5Cl(g)} + \mathrm{CH_3COCl(l)}$$

and the kinetic rate law is given by

$$r_1 = A_1 \exp\left(\frac{-E_1}{R_g T}\right) C_s C_A C_B \tag{22}$$

Eq. (22) is largely in conformity with the effective rate equation proposed by the authors [10] on the basis of a radical mechanism. The particle population balance, Eq. (2), along with the 'linear' dissolution rate, Eq. (1), given in Section 2 remaining as they are, the pertinent liquid side balance equations would be as follows

$$V_l \frac{dC_s}{dt} = \sum_{D_{PL}}^{D_{PH}} k_{ls} a_{ls} (C_s^* - C_s) - V_l r_1 \tag{23}$$

$$\frac{dC_A}{dt} = \frac{dC_B}{dt} = -r_1 \tag{24}$$

$$\frac{dT}{dt} = \frac{(-\Delta H_r) V_l r_1}{m_s c_{vs} \phi} \tag{25}$$

with the initial concentration of the solute $C_s = 0$, those of the liquid phase species A and B being C_{A0} and C_{B0} and the initial temperature set at close to the ambient one, T_0. ΔH_r is the heat of reaction (−ve sign implying exothermicity). m_s is the mass of the reactor contents (inclusive of the solid charge) and c_{vs} is the constant volume specific heat of the same. ϕ is the thermal inertia defined as

$$\phi = 1 + \frac{m_b c_{vb}}{m_s c_{vs}} \tag{26}$$

Eq. (25) is the type of heat balance equation commonly used in the analysis and interpretation of data from adiabatic calorimeters and small-scale reactors [26] and allows one to calculate the maximum possible (adiabatic) temperature rise. Eqs. (23)–(25) were solved simultaneously with the Eq. (2) along with the ancillary Eqs. (1), (5), (6), (22) and (26). The solution procedure was exactly the same as discussed in Section 2.

In an experiment described by Wang et al. [10], to a mixture of thionyl chloride and ethyl acetate (liquid volume 10^{-4} m^3) with specified composition, 0.02 kg of zinc powder (with a particle size range 50–75 μm) was charged at the ambient temperature. An exothermic reaction with intense self-heating occurred after about 14 min of storage. A peak temperature of 163.8 °C was recorded. A lot of gas evolution also took place with attendant pressure rise. The model was used to simulate the temperature rise as observed in the above experiment.

As in the case of TPA conversion experiments considered in the previous case, we assumed an initial particle size distribution given by the Eq. (14) with the parameters n and $\overline{D}$ chosen ($n = 26$, $\overline{D} = 68.5$ μm) so as to start with a fairly narrow distribution having a particle size range as specified. Although not mentioned, we assumed an agitation speed same as that would be required for complete suspension of the particulate phase. Once these two parameters were chosen, Eq. (8) was used to calculate the appropriate values for k_{ls} at all stages of calculation. The pure component properties of zinc, thionyl chloride and ethyl acetate were taken from the handbooks [22,23]. The required specific heat, density and viscosity of the liquid phase were calculated given the liquid composition, diffusivity calculated by the same correlation as used in the earlier problem. The property values used in the simulation have been summarized in the upper part of Table 3. The same table also presents the values for the activation energy and the heat of reaction. These were the same as reported by Wang et al. [10].

Table 3
Input data and the predicted results for the thermal runaway during dissolution of metallic zinc powder in a liquid mixture of thionyl chloride (43%, v/v) and ethyl acetate (57%, v/v)

Quantities	
Input data	
Liquid volume (m^3)	1.0×10^{-4}
Liquid density (kg m^{-3})	1.214×10^3
Liquid viscosity (m Pa s)	0.507
Liquid specific heat (kJ (g K)$^{-1}$)	1.354×10^{-3}
Zn loading (kg)	0.02
Particle size range of Zn powder (μm)	50–75
Starting temperature (°C)	26
Heat of reaction (kJ mol^{-1})	125.5
Activation energy (kJ mol^{-1})	83.68
Frequency factor	3.25×10^{10}[a]
Thermal inertia	1.68[a]
Predicted quantities	
Final adiabatic temperature (°C)	163.1
Maximum self-heat rate (°C min^{-1})	267
Temperature at the maximum rate (°C)	122.8
Time-to-maximum rate (min)	14.37

[a] Estimated in the present work.

The thermal inertia of the calorimeter/reactor and the frequency factor in the reaction rate equation, Eq. (22), were the two parameters that were estimated (see Table 3) to simulate the experimental temperature rise data. The same parameter estimation technique as used in the earlier problem was used successfully. The former affects the adiabatic temperature rise and the latter controls the onset of self-heating. It is seen from the lower part of Table 3 that both the peak temperature and the TMR (as observed in experiment) have been almost exactly predicted by the model. Fig. 6 compares the predicted temperature rise profile with the experimental data (recorder trace). The plots are remarkably close validating the model and the estimated parameters.

In actual applications, the bomb or the calorimeter heat capacity is likely to be known or measurable, thereby assigning an appropriate value for the thermal inertia. The only unknown in that case would have been the Arrhenius parameters. The model presented here can be used to estimate these parameters to fit a measured temperature profile.

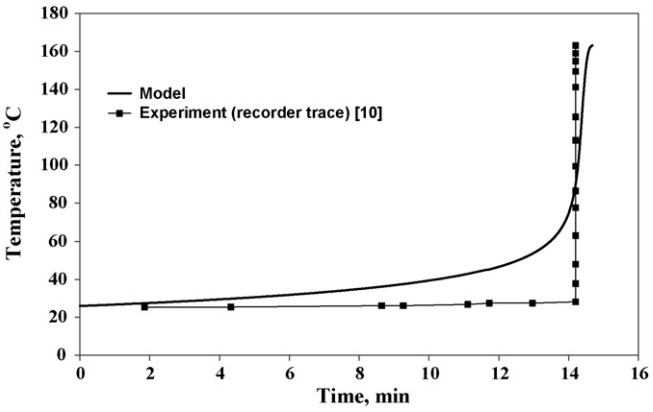

Fig. 6. Predicted temperature rise in the reaction between metallic zinc and thionyl chloride-ethyl acetate mixture.

4.2. Effect of particle size and poly-dispersity on the self-heating rate

For a two-phase reaction system exhibiting thermal runaway such as the one studied above any process or operating parameter that affects the runaway characteristics like TMR and/or the maximum self-heat rate would be of great interest. Particle size is obviously an important choice in this regard inasmuch as that could affect the rate of mass transfer, which in turn could have a bearing on the rate of temperature rise. Through out this work we consistently proposed to specify the charge by both the mean particle size and the extent of poly-dispersity. In what follows we show the effect of both on several quantities of interest by numerical case studies using the model.

In Table 4 seven rows of results have been listed. In all cases maximum self-heat rate, TeMR and TMR have been reported. Case nos. 1, 2 and 5 show the effect of changing $\overline{D}$ maintaining the same value for n. The cases 3–7, on the other hand, show the effect of changing n at the same $\overline{D}$. In each case we have also calculated the mean particle size, D_m (which is usually smaller than $\overline{D}$), by the formula given in Eq. (21).

As expected, on reducing the mean particle size, keeping the same poly-dispersity (cases 1, 2 and 5), the rate of reaction increases significantly, which is directly reflected in the increase in maximum self-heat rate. However, when the reduction of the mean particle size is accompanied with the increase in the poly-dispersity (by progressively reducing n in the cases, 3–7), the peak self-heat rate at first increases, goes through a maximum at moderate n before going down again for more highly poly-disperse charges. In this case, the rate-enhancing effect of reduction in the mean particle size is at first partly compensated for and, eventually, fully overtaken by the deleterious effect of increasing the poly-dispersity of the charge. Here we show that, though quantitatively marginal under the specified conditions, poly-dispersity may also modulate the rate and the heat generation. This result does not seem to have been reported before and could not have been foreseen in studies discounting the poly-dispersity of the solid phase. Interestingly, the TMR remained almost the same in all the seven cases. The onset of the self-heating and the TMR directly depends on the kinetic factors which can be easily demonstrated by changing the value of the frequency factor. The activation energy has an even more dramatic effect.

5. Extension of the model to a complex reaction system: solid–liquid phase-transfer catalysis

5.1. The conceptual background and the context

In conducting a variety of organic synthesis reactions between the reagents that are normally in mutually insoluble phases, small amounts of phase-transfer agents or catalysts (PTC) like quaternary ammonium or phosphonium salts or crown ethers have been known [27] to facilitate the reactions under mild conditions and sometimes enhance the rate significantly. For example, a very slow nucleophilic substitution such as the cyanide displacement on an alkyl chloride like chlorooctane (RX) dissolved in an organic solvent is enhanced by addition of a small amount of tetrabutyl ammonium chloride (a quaternary ammonium salt, Q^+X^-). The latter forms an ion-pair with the nucleophile (the cyanide ion, Y^-) in the aqueous phase and is sufficiently lipophilic as well for the same ion pair (Q^+Y^-, the active form of the PTC) to be extracted into the organic phase where the displacement reaction can then take place and the product cyano-octane (RY) is formed. The regenerated PTC redissolves into the aqueous phase and the non-reactive chloride anion is again exchanged for the reactive cyanide anion.

In the above example, the aqueous phase serves both as a source of the nucleophile (cyanide) and as a sink for the non-reactive product anion (chloride), with the PTC mediating the cyanide for chloride ion-exchange in the aqueous phase. In some cases it is possible to replace the aqueous solution with the solid salt (such as sodium cyanide in the above example) for substan-

Table 4
Effect of particle size and the poly-dispersity on the self-heating rate during dissolution of metallic zinc powder in a liquid mixture of thionyl chloride (43%, v/v) and ethyl acetate (57%, v/v)

Case no.	n	$\bar{D}$ (μm)	Size range (μm)	D_m (μm)	Maximum rate (°C min^{-1})	TeMR (°C)	TMR (min)
1	9	85	33–110	81.6	214.9	120.0	14.28
2	9	62.5	25–81	60.0	301.1	125.0	14.22
3	26	45	32–50	44.4	423.9	130.0	14.52
4	15	45	25–53	43.9	426.4	130.0	14.51
5	9	45	18–58	43.2	427.3	129.4	14.31
6	7	45	13–63	42.7	426.7	129.4	14.37
7	5	45	7–70	41.8	415.2	127.7	14.81

tially the same duty. Conducting such a reaction in an anhydrous manner (usually termed as solid–liquid phase-transfer catalysis reaction or SLPTC) may have commercial advantages [28], the most important among them being the elimination of undesirable side reactions that water may promote in some cases, as well as the ease of product separation. The issue of natural barrier for the transport of the nucleophile between the solid and the liquid phases being still the key problem, the challenge is to have the PTC, dissolved in the organic phase, to somehow mediate the above ion-exchange, either on the solid surface (*heterogeneous solubilisation*) or in the liquid phase (*homogeneous solubilisation*) close to the solid–liquid interface [29,30].

Many examples of SLPTC reactions have been reported in the literature [28], which may approximate one or the other categorization as above with good reason, a full discussion of which is beyond the scope of the present paper. It has been suggested [28] that for the quaternary salts wherein the positive charge is effectively shielded by the large alkyl groups there would be steric hindrance for the PTC to approach the solid surface too closely and hence direct solubilsation from the surface may be generally discounted. In that case homogeneous solubilisation is the likely mechanism, wherein the nucleophilic solid would have a small but finite solubility in the organic phase.

Fig. 7 is a schematic diagram that depicts the inter-phase diffusional transport mediating the dissolution of a spherical particle of MY into an organic solvent which contains the substrate RX and the phase-transfer catalyst QX pre-dissolved in it. As MY diffuses into the liquid film intervening between the particle and the bulk liquid phase, it participates instantaneously in the reversible ion-exchange reaction with QX diffusing in the opposite direction from the bulk phase into the film. The resulting ion-pair QY diffuses out into the bulk phase and reacts with RfX to produce the desired product RY while re-generating QX, which in turn would diffuse back into the film thus completing the PTC reaction cycle. Considering that the solubility of the salt in the organic solvent would be generally extremely small it may not be inappropriate to assume that the concentration of MY in the bulk phase is negligible and that there is no flux of MY from the film into the bulk. The concentration profiles of all the three species conforming to the above picture are schematically shown in Fig. 7.

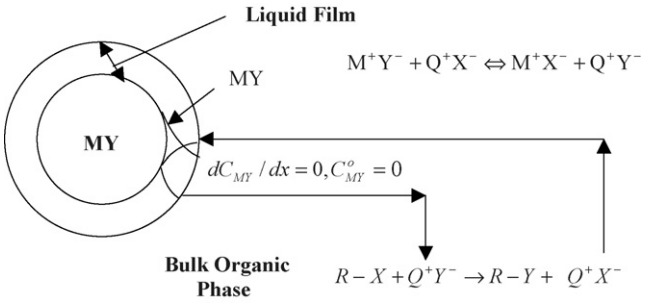

Fig. 7. Schematic diagram of the inter-phase transport of the solid salt MY into the organic phase accompanied with the reactions in the film and the bulk.

The above scheme is conceptually very similar to the model D among the four mechanistic schemes discussed by Naik and Doraiswamy [30] for homogeneous solubilisation in SLPTC reactions. Our scheme is distinguished from their model in the following respect apart from the consideration of a poly-disperse solid reactant. We have assumed that only the ion-exchange takes place inside the film and the bimolecular displacement reaction takes place in the bulk liquid phase, and furthermore that the ion-exchange is an instantaneous reversible reaction. In kinetic studies of mass transfer controlled PTC reactions [31] such ion-exchange equilibria have been assumed over the entire liquid phase including the film adjoining the interface. In the light of the significant mass transfer control of the overall rate that is discernible from the observed data to be discussed shortly, the above assumptions seemed justified and led to useful simplification of the treatment.

Pradhan and Sharma [9] had conducted phase-transfer catalysed sulfidation of benzyl chloride. In the typical experimental protocol, benzyl chloride and a quaternary ammonium salt (TBAB) dissolved in toluene were charged into a laboratory mechanically agitated glass reactor, which included a six-bladed glass disk turbine impeller with appropriate clearing at the bottom, also provided with a stainless steel cooling coil. Sodium sulfide particles of a specified size range were charged into the reactor and the mixture stirred at a particular agitation speed. The reactor was kept under isothermal conditions. From the observed marginal effect of temperature (an activation energy of about 9.6 kJ/mol) the mass transfer control of the measured rate of reaction was suggested. In a clear demonstration of this conjecture, experiments conducted with three size cuts of the sodium sulfide particulate charge showed an inverse square dependence of the rate on the mean particle size. We tried to simulate these results using our model after an appropriate extension.

5.2. Model extension

To adapt the model (see Section 2) to this class of reactions, we would primarily need a redefinition of the 'linear' dissolution rate $R(D_P)$ to be used in the particle population balance, Eq. (2). We would also need to write a set of mass balance equations for the concentration of the species RX, RY, QY and QX in the organic phase reflecting the inter-phase transport of the quaternary ion-pairs.

Solution has been given [32] for the mathematical model of absorption of a gaseous solute followed by an instantaneous reversible reaction with a dissolved reactant. By analogy, for the particular bimolecular 4-species reversible reaction (the ion-exchange) as we are concerned with in this paper along with the zero flux assumption as above, it can be shown that the intrinsic particle dissolution rate is given by

$$R(D_P) = \frac{dD_P}{dt} = -\frac{2MW_s k_{ls} C^*_{MY}[1 + (D_{QY}/D_{MY})\Phi/C^*_{MY}]}{\rho_s} \quad (27)$$

where

$$\Phi = 0.5\left\{\left[\left(\frac{D_{MX}}{D_{QX}}\right)K_{QY}C^*_{MY}\right]^2 + 4K_{QY}C^*_{MY}\left(\frac{D_{MX}}{D_{QY}}\right)C^o_{QX}\right\}^{0.5} - 0.5\left(\frac{D_{MX}}{D_{QX}}\right)K_{QY}C^*_{MY} \quad (28)$$

From the same analysis the expressions for the fluxes of QY out and that of QX into the film can also be written. Using the generalized kinetic model framework for the mass transfer controlled PTC reactions developed earlier by us [33] the pertinent liquid phase balance equations can be written as

$$\frac{dC^o_{RX}}{dt} = -k_2C^o_{RX}C^o_{QY} \quad (29)$$

$$\frac{dC^o_{RY}}{dt} = k_2C^o_{RX}C^o_{QY} \quad (30)$$

$$\frac{dC^o_{QY}}{dt} = -k_2C^o_{RX}C^o_{QY} + \sum_{D_{PL}}^{D_{PH}}\frac{k_{ls}a_{ls}C^*_{MY}[1+(D_{QY}/D_{MY})\Phi/C^*_{MY}]}{V_l} \quad (31)$$

$$\frac{dC^o_{QX}}{dt} = k_2C^o_{RX}C^o_{QY} - \sum_{D_{PL}}^{D_{PH}}\frac{k_{ls}a_{ls}C^*_{MY}[1+(D_{QY}/D_{MY})\Phi/C^*_{MY}]}{V_l} \quad (32)$$

where a_{ls} would be calculated by the Eqs. (5) and (6) and k_{ls} has to be obtained using a suitable correlation as in the previous problems. The initial conditions are:

$$C^o_{RX} = C_{RX0} \quad (33)$$

$$C^o_{QX} = C_{QX0} \quad (34)$$

$$C^o_{RY} = C^o_{QY} = 0 \quad (35)$$

The above is the complete set of extended model equations, which can be solved for predicting the rate of consumption of the organic phase reactant, R_{RX}, a quantity which was measured experimentally.

5.3. Comparison with experimental data

Consistent with the species nomenclature used in this section, the sulfide anion is represented by Y, the leaving anion (chloride) by X, the tetrabutylammonium cation by Q, the organic phase reactant benzyl chloride by RX and the sodium sulfide salt by MY. Table 5 summarises all the necessary input data in order to apply the model to this problem. Most of the process and operating data have been taken from the description given by Pradhan and Sharma [9] as under their Fig. 2. The pure component properties have been taken from the standard handbooks. The salt solubility is expected to be very low, ion-exchange equilibrium constant reasonably large, neither value having been reported. We used the values as used by Naik and Doraiswamy [30] for a similar problem. The sensitivity of the calculated rates towards these parameters was found negligible. The base value of diffusivity of the salt was estimated by using Wilke–Chang correlation. Those for QY and QX can also be estimated assuming them to be neutral molecules, but the values are not quite reliable. In absence of measured data or proper estimates, the diffusivity ratios along with the bimolecular rate constant k_2 for the displacement reaction were estimated which allowed model predictions to best fit the observed rate values for varying mean particle size for the particulate charges used in experiments. The finally estimated values have been reported in Table 5.

Table 5
Input data for predicting the rate of TBAB catalysed sulfidation of benzyl chloride

Quantities	
Input data	
Liquid volume (m^3)	3×10^{-4}
Concentration of benzyl chloride (kmol m^{-3})	1.25
Concentration of TBAB (kmol m^{-3})	2.5×10^{-3}
Solid Na_2S loading (kg m^{-3})	10^2
Speed of agitation (rpm)	2000
Particle size ranges (three cuts; μm)	
1	106–500
2	500–850
3	1003–1404
Diffusivity ratios	
D_{QY}/D_{MY}	1.0
D_{QX}/D_{MX}	0.357
D_{QY}/D_{QX}	3.08
Solid Solubility (kmol m^{-3})	5×10^{-2}
Displacement rate constant (m^3 $kmol^{-1}$ s^{-1})	0.475
Ion-exchange equilibrium constant	10
Conversion (%)	40

As with the other problems dealt with in this paper, the poly-disperse particulate charges were represented by the Rosin–Rammler distribution with appropriate values for the parameters n and $\bar{D}$ so as to match the specified size ranges (see Table 6). The corresponding mean particle sizes were calculated by the formula given in the Eq. (21). This is clearly more appropriate than the values quoted by Pradhan and Sharma [9] that were obtained by computing mere arithmetic average of the limiting values for a given size range. The predicted rates appear in the last column of this table. Fig. 8 shows a close approximation by the model predictions of the inverse squared dependence

Table 6
Effect of particle size and poly-dispersity of the solid Na_2S charge on the rate of TBAB catalysed sulfidation of benzyl chloride (at a matching conversion of 40%)

Case no.	n	$\bar{D}$ (μm)	Size range (μm)	D_m (μm)	$R_{RX} \times 10^5$ (kmol m^{-3} s^{-1})
1	7	360	102–496	342	65.82
2	21	750	498–838	737	22.91
3	31	1300	982–1402	1285	8.42

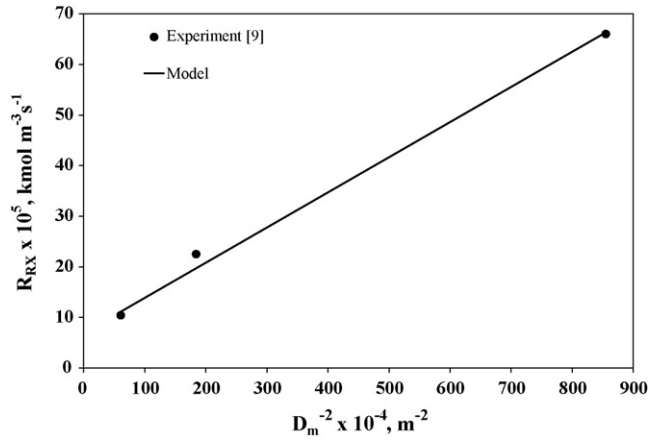

Fig. 8. Effect of particle size on the rate of TBAB catalysed sulfidation of benzyl chloride.

of the observed rate on the mean particle size of the charge (a clear indication of the mass transfer control of the rate). This fit justified the assumption of $Sh_p = 2$ for this data set (surmised correctly by Pradhan and Sharma [9]) and estimation of k_{ls} on this basis.

6. Conclusions

In the foregoing a general-purpose model has been presented which successfully simulates experimentally observed integral batch reactive dissolution rate data while accounting for the specified poly-dispersity of the solid particulate charge. The applicability of the model was shown to be spanning from a simple isothermal reaction to an exothermic reaction with runaway potential and to a phase-transfer catalysis reaction with a complex mechanism. We believe that it can be applied to many more solid–liquid reaction systems of interest in organic synthesis, provided the reaction kinetic scheme is broadly known and can be schematically represented. The model and the adjunct numerical calculation procedure, consciously designed to achieve this versatility with minor modifications and extensions, should help practitioners in the organic chemical process research and development.

The model was shown to predict the time required for a specified extent of conversion of the particulate reactant or the rate of consumption of a key liquid reactant under a variety of process and operating conditions, like temperature, liquid reactant and the catalyst concentration, agitation speed, particle size and poly-dispersity of the charge. Such information is useful in reactor design and scale-up. Where dissolution is accompanied with exothermic and gas producing reaction with runaway potential, the model can be used to predict quantities of interest in hazard assessment and should aid safe reactor design. The effect of poly-dispersity of the solid phase on the rate of reaction in general and heat generation, in particular, in exothermic reactions, has been predicted by the model, to the best of our knowledge for the first time and may presage useful applications after careful experimental verification in future.

References

[1] G.V. Sidorov, S.S. Gluzman, V.M. Ivanova, E.L. Vulakh, Application of the method of kinetic invariants to the description of a multiphase process of organic synthesis, J. Appl. Chem. USSR 58 (1986) 1781–1784.
[2] A. Loupy, P. Pigeon, M. Ramdani, Synthesis of long chain aromatic esters in a solvent-free procedure under microwaves, Tetrahedron 52 (1996) 6705–6712.
[3] J.M. Lee, J.R. Donofrio, Copper leaching from chalcopyrite in hydrochloric acid, AIChE Symp. Ser. 78 (216) (1982) 116–126.
[4] S. van der Sluis, Y. Meszaros, W.G.J. Marchee, H.A. Wesslingh, G.M. van Rosmalen, The digestion of phosphatic ore in phosphoric acid, Ind. Eng. Chem. Res. 26 (1987) 2501–2505.
[5] A. Yartasi, M.M. Kocakerim, S. Yapici, C. Ozmetin, Dissolution kinetics of phosphate ore in SO_2-saturated water, Ind. Eng. Chem. Res. 33 (1994) 2220–2225.
[6] L. Bernard, M. Freche, J.L. Lacout, B. Biscans, Modeling of the dissolution of calcium hydroxide in the preparation of hydroxyapatite by neutralization, Chem. Eng. Sci. 55 (2000) 5683–5692.
[7] S.E. Leblanc, H.S. Fogler, Population balance modeling of the dissolution of polydisperse solids: rate limiting regimes, AIChE J. 33 (1987) 54–63.
[8] A. Bhattacharya, Predicting rates of dissolution of polydisperse solids in reactive media, Chem. Eng. Proc. 46 (2007) 573–583.
[9] N.C. Pradhan, M.M. Sharma, Kinetics of reactions of benzyl chloride/*p*-chlorobenzyl chloride with sodium sulfide: phase-transfer catalysis and the role of the omega phase, Ind. Eng. Chem. Res. 29 (1990) 1103–1108.
[10] S.S.Y. Wang, S. Kiang, W. Merkl, Investigation of a thermal runaway hazard drum storage of thionyl chloride/ethyl acetate mixture, Proc. Safety Prog. 13 (1994) 153–158.
[11] T.N. Zwietering, Suspending of solid particles in liquid by agitators, Chem. Eng. Sci. 8 (1958) 244–253.
[12] A.W. Nienow, Suspension of solid particles in turbine agitated baffled vessels, Chem. Eng. Sci. 23 (1968) 1453–1459.
[13] P. Harriot, Mass transfer to particles: Part I. Suspended in agitated tank, AIChE J. 8 (1962) 93–102.
[14] P.H. Calderbank, M. Moo-Young, The continuous phase heat and mass transfer properties of dispersions, Chem. Eng. Sci. 16 (1961) 39–54.
[15] V.G. Levich, Physicochemical Hydrodynamics, Prentice-Hall, Englehood Cliffs, NJ, 1962, pp. 176–183.
[16] D.N. Miller, Scale-up of agitated vessels, Ind. Eng. Chem. Proc. Des. Dev. 10 (1971) 365–375.
[17] P.M. Armenante, D.J. Kirwan, Mass transfer to microparticles in agitated systems, Chem. Eng. Sci. 44 (1989) 2781–2796.
[18] C.K. Batchelor, The Theory of Homogeneous Turbulence, Cambridge University Press, Cambridge, 1960, pp. 1–115.
[19] A.W. Nienow, Dissolution mass transfer in a turbine agitated baffled vessel, Can. J. Chem. Eng. 47 (1969) 248–258.
[20] A. Adrover, A. Velardo, M. Giona, S. Cerbelli, F. Pagnanelli, L. Toro, Structural modelling for the dissolution of non-porous ores: dissolution with sporulation, Chem. Eng. J. 99 (2004) 89–104.
[21] P. Ditl, J. Sestak, K. Partyk, Mass-transfer kinetics in dissolving polydisperse solid materials, Int. J. Heat Mass Transfer 19 (1976) 635–641.
[22] R.H. Perry, D.W. Green, J.O. Maloney (Eds.), Perry's Chemical Engineers' Handbook, seventh ed., McGraw-Hill, New York, 1997, pp. 7–374 (Section 2).
[23] D.R. Lide (Ed.), CRC Handbook of Chemistry and Physics, 85th ed., CRC Press, Boca Raton, 2004, pp. 4–88 (Section 4).
[24] R. Reid, J.M. Prausnitz, T.K. Sherwood, The Properties of Gases and Liquids, third ed., McGraw-Hill Book Company, New York, 1977, pp. 658–732.
[25] J.L. Kroschwitz, M. Howe-Grant (Eds.), Kirk-Othmer Encyclopedia of Chemical Technology, vol. 18, fourth ed., John Wiley and Sons, New York, 1996, pp. 1006–1007.
[26] J.C. Leung, H.K. Fauske, H.G. Fisher, Thermal runaway reactions in a low thermal inertia apparatus, Thermochim. Acta 104 (1986) 13–29.
[27] C.M. Starks, R.M. Owens, Phase-transfer catalysis. II. Kinetic details of cyanide displacement on 1–Halooctanes, J. Am. Chem. Soc. 95 (1973) 3613–3617.

[28] H.A. Lee, H.J. Palmer, S.H. Chen, Solid–liquid phase transfer catalysis, Chem. Eng. Progr. (February) (1987) 33–39.
[29] J.B. Melville, J.D. Goddard, A solid–liquid phase transfer catalysis in rotating-disk flow, Ind. Eng. Chem. Res. 27 (1988) 551–555.
[30] S.D. Naik, L.K. Doraiswamy, Mathematical modeling of solid–liquid phase-transfer catalysis, Chem. Eng. Sci. 52 (1997) 4533–4546.
[31] S. Asai, H. Nakamura, Y. Furuichi, Alkaline hydrolysis of *n*-butyl acetate with phase-transfer catalyst aliquat 336, AICHE J. 38 (1992) 397–404.
[32] P.V. Dancwerts, Gas–Liquid Reactions, McGraw-Hill Book Company, New York, 1970, pp. 130–131.
[33] A. Bhattacharya, A. Mungikar, Kinetic modelling of mass transport limited phase transfer catalysed reactions, J. Mol. Catal. A: Chem. 181 (2002) 243–256.